Journal of Materials Chemistry A

Accepted Manuscript

ROYAL SOCIETY OF CHEMISTRY

www.rsc.org/materialsA

Cite this: DOI: 10.1039/c0xx00000x

www.rsc.org/xxxxxx

ARTICLE TYPE

Preparation and properties of thermostable well-functionalized graphene oxide/polyimide composite films with high dielectric constant, low dielectric loss and high strength via *in situ* polymerization

Xinliang Fang[a], Xiaoyun Liu[a], Zhong-Kai Cui[b], Jun Qian[a], Jijia Pan[a], Xinxin Li[a],Qixin Zhuang*[a]*

Received (in XXX, XXX) Xth XXXXXXXXX 20XX, Accepted Xth XXXXXXXXX 20XX
DOI: 10.1039/b000000x

This study proposes a novel and facile method to synthesize high-quality NH_2-functionalized and carboxyl-functionalized graphene oxide (PPD-CFGO)/polyimide (PI) composite films with high dielectric constant (ε), low dielectric loss, high-temperature resistance and outstanding mechanical properties by *in situ* polymerization. In addition to partial carboxyl groups located at the edges, the ample hydroxyl and epoxy groups bonded on the basal plane of graphene sheets were exploited to covalently bond to the amines. GO was modified by oxalic acid to obtain carboxyl-functionalized GO (CFGO) before amidation. NH_2-functionalized CFGO (PPD-CFGO), dispersing well in dimethylacetamide (DMAc), was the initial platform for polymer grafting to improve CFGO dispersion in the polymer matrix. Partially reduced graphene nanosheets are formed during the imidization process. The PPD-CFGO/PI composite films exhibit high tensile strength (up to 848 MPa) and Young's modulus (18.5 GPa). The thermogravimetric analyses results indicate that the PPD-CFGO/PI composites have good thermal stability below 500 ℃. The dielectric constant increases up to 36.9 with increasing amount of PPD-CFGO, higher than that of the pure PI polymer by a factor of 12.5, while the dielectric loss is only 0.0075 and the breakdown strength still remains at a high level (132.5±9.3 MV/m).

Introduction

With the development of solar and wind power, energy storage technologies are essential for efficient utilization of electricity generated from these renewable sources.[1, 2] Compared to other energy storage technologies, capacitors possess the intrinsic advantage of high power density due to their fast charge and discharge capability. Advances in capacitors are highly dependent on the development of dielectric materials with high permittivity (ε).[3] Polymers are more applicable than inorganic ceramics in higher electric fields.[4] However, further development of polymer dielectrics are challenged by high operating temperature. For instance, the limit of working temperature of biaxially oriented polypropylene polymer-based capacitors is 105 ℃.[5] Therefore, high-temperature resistance materials with high dielectric constants are desirable for applications at high temperature. Polyimides (PIs) are considered to be one of the most important high performance materials due to their superior mechanical properties, high glass transition temperature, excellent thermal stability and good resistance to solvents.[6-8] PI starts to decompose at approximately 600 ℃. Thus, PI is suitable to be employed in the dielectric field as a high-temperature resistant polymer matrix.

Usually there are two approaches for increasing the dielectric constant of the polymer. One is introducing high-k ceramic fillers, such as nano-TiO_2,[9] Al_2O_3,[10] $BaTiO_3$[11-13] and $CaCu_3$-Ti_4O_{12},[14, 15] into the polyimide matrix. However, to get a higher dielectric constant, the mechanical properties and the process ability of composite films will be dramatically reduced, owing to the too much introduction of ceramic fillers. The other approach for raising the ε value is to incorporate electrically conductive particles into polymers to form percolated composites based on percolation theory.[16, 17] This strategy involves the creation of the so-called microcapacitor networks in the matrix at the percolation threshold to gain a distinctly enhanced ε_r value.[18] Chen et al.[19] added multi-wall carbon nanotubes (MWNT) into polyimide to obtain MWNT/PI composite films with high dielectric constant (31.3) at a relatively high percolation threshold (m_c = 10%).

Graphene, a unique atomically thick 2D nanocarbon material, has attracted considerable attentions due to its extraordinary thermal, electric and mechanical properties.[20-23] A lot of relevant studies have been done based on graphene in the matrix of polyaniline,[24] poly(vinylidene fluoride),[25, 26] Carboxylated nitrile rubber,[27] etc. Moreover, the temperature resistance and mechanical properties of the graphene/polymer composites remain the same or even much better, instead of getting worse. Wang et al.[28] and Liao et al.[29] reported graphene oxide/polyimide composites with low dielectric constant, high-temperature resistance and outstanding mechanical properties. Luong et al.[30] also reported graphene/polyimide composites with good mechanical and electrical properties. And Yang et al.[31] reported poly(vinylidenefluoride-*co*-hexafluoro propylene) based nanocomposites filled with fluoro-polymer functionalized RGO.

In order to reinforce graphene/polymer nanocomposites, two basic problems must be considered: (1) dispersion of graphene in

(a). Key Laboratory of Specially Functional Polymeric Materials and Related Technology, Ministry of Education, School of Materials Science and Engineering, East China University of Science and Technology, Shanghai 200237, China
(b). Department of Chemistry, Université de Montréal, C.P. 6128, Succ. Centre Ville, Montréal, Québec, Canada, H3C 3J7

the polymeric matrix, and (2) the interfacial interactions between graphene and polymer. However, it is hard to gain a good dispersion of graphene in polymeric matrices. Graphene-based materials, such as graphene nanoplatelets (GNPs), graphene nanosheets (GNSs) and graphene oxide (GO), exhibit great potential for improving the properties of polymers due to their extremely high aspect ratio, high conductivity, unique graphitized planar structure and low manufacturing cost.[32-34] As a result of its unique chemical structures, GO shows the widest potential for further functionalization among those graphene-based materials.[35, 36]

In addition to partial carboxyl groups located at the edges, heavily oxygenated graphene oxide sheets possess abundant hydroxyl and epoxy groups bonded on the basal planes. However, most previous studies on graphene-based composites only utilized the edged carboxyl groups to bond amino-groups, leaving plenty of oxygenated groups intact,[37, 38] which means that polymer chains are attached at the edges rather than being fixed to the basal planes. In order to make full use of oxygen functional groups, we transformed the hydroxyl and epoxy groups to carboxyl groups by using concentrated hydrobromic acid (HBr) and oxalic acid (HOOC-COOH) and obtained carboxyl-functionalized graphene oxide (CFGO).[39] Then, CFGO was modified by p-phenylenediamine (PPD) to gain NH_2-functionalized CFGO (PPD-CFGO) with N,N′-dicyclohexylcarbodiimide (DCC) as the catalyst.[23] The ultimate functionalized graphene nanoparticles were introduced into the polymeric matrix to form PPD-CFGO/PI composites by *in situ* polymerization. Since the polymer chains are fixed to the basal planes, graphene oxide sheets are separated effectively to prevent irreversible agglomerations, which is beneficial for the dispersion and formation of microcapacitor networks in the matrix, resulting in good dielectric and mechanical properties. To the best of our knowledge, this is the first report of graphene/polyimide composites with high dielectric constant (ε), low dielectric loss, high-temperature resistance and outstanding mechanical properties at a low percolation threshold.

Experimental section

Materials

Graphite powder was purchased from Alfa Aesar (Massachusetts, USA). p-Phenylenediamine (PPD) and 4,4′-diaminodiphenyl ether (ODA) were obtained from Aladdin (Shanghai, China). Pyromellitic dianhydride (PMDA) was provided by J & K (Beijing, China). Reagents including sodium nitrate ($NaNO_3$), sulfuric acid (H_2SO_4), potassium permanganate ($KMnO_4$), hydrogen peroxide (H_2O_2), hydrobromic acid (HBr), oxalic acid, dimethylacetamide (DMAc), N,N-dimethylformamide (DMF) and N,N′-dicyclohexylcarbodiimide (DCC), were supplied by Aldrich Chemical Company (Milwaukee, USA). DMAc was dried with calcium hydride (CaH_2) prior to distillation. Other reagents were of high purity and used as received.

Synthesis of carboxyl-functionalized graphene oxide (CFGO)

0.075 g GO, prepared according to the process reported by Hummers and Offeman,[40] was dispersed in 30 mL de-ionized water under ultrasonication for 0.5 h. 0.04 mol HBr was added and vigorously stirred for 24 h. Then, 1.50 g oxalic acid was added and stirred for another 4 h. The dispersion was filtrated and dried at 50 ℃ under vacuum for 24 h.

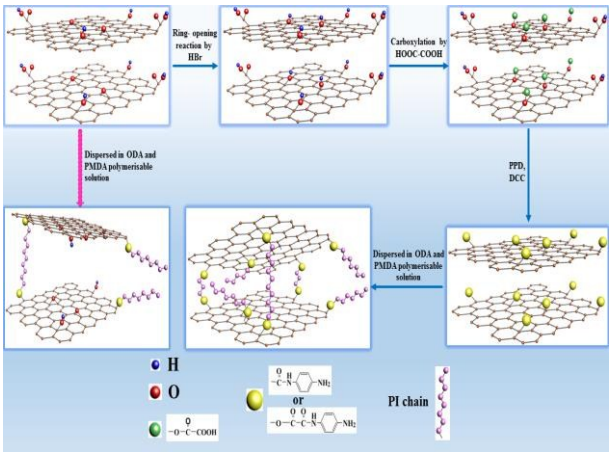

Scheme.1 Synthesis of PPD-CFGO/PI composite films.

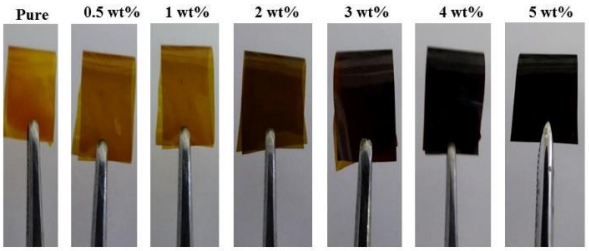

Fig.1 Images of PPD-CFGO/PI composite films.

Preparation of PPD-GO and PPD-CFGO

0.05 g GO or CFGO was dispersed in 20 mL DMAc by ultrasonication for 0.5 h before adding PPD (0.05 g, 0.46 mmol) and DCC (0.05 g, 24 mmol). The dispersed solution was stirred for 24 h under nitrogen purge at room temperature. The mixture was filtrated and washed with DMF and ethanol. The sample of PPD-GO or PPD-CFGO was obtained after drying at 60 ℃ in a vacuum oven for 24 h.

Preparation of PPD-GO/PI films via *in situ* polymerization process

10.45 mg PPD-CFGO was dispersed in anhydrous DMAc (20 mL), using tip sonication (0.5 h), leading to a stable dispersed solution. Then ODA (1.00 g, 5 mmol) was added and the mixture was stirred at room temperature under nitrogen purge. When ODA was completely dissolved in the DMAc, PMDA (1.09 g, 5 mmol) was divided equally into four batches and was added to the mixed solution by batch every 1 h. Once PDMA was completely dissolved in the DMAc, the solutions were stirred for 24 h and then poured into a glass dish. After natural drying for 48 h, the sample was put into an air-circulated oven at 100, 200 and 300 ℃ for 2 h, respectively and 400 ℃ for 5 min. Finally, PPD-CFGO/PI composite films containing 0.5 wt%, 1 wt%, 2 wt%, 3 wt%, 4 wt% and 5 wt% of PPD-CFGO were prepared.

Characterization

The thickness of the GO and PPD-CFGO nanosheets was measured by atomic force microscopy (AFM, NanoScope IIIa).

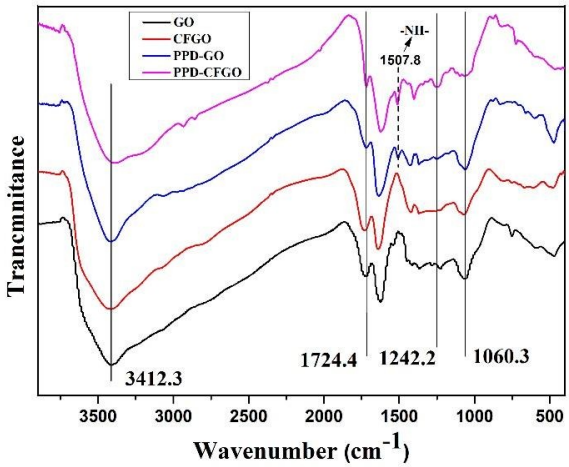

Fig.2 FTIR spectra of GO, CFGO, PPD-GO and PPD-CFGO.

Samples were prepared by depositing the homogeneous aqueous GO and PPD-CFGO solutions onto a fresh mica plane. Fourier-transformed infrared spectra (FT-IR, Nicolet Magna-IR 550) were acquired using pressed KBr pellets. Raman spectra were taken on a Renishaw in Via Reflex Raman spectrometer with a backscattering configuration at 514 nm. X-ray diffraction (XRD) analysis was carried out on a D/MAX 2550 VB/PC rotating anode X-ray multicrystal diffraction spectrometer equipped with Ni-filtered Cu Ka radiation and operated at 60 mA and 40 kV. X-ray photoelectron spectroscopy (XPS) was carried out in a thermo scientific ESCALAB 250Xi X-ray photoelectron spectrometer equipped with amonochromatic Al Ka X-ray source (1486.6 eV). The fractured surface of the specimen was analysed using field-emission scanning electron microscopy (FESEM, Hitachi S-4800). The morphologies of GO, CFGO and PPD-CFGO were characterized by the high-resolution transmission electron microscopy (HRTEM, JEOL JEM-2100). Tensile property values reported here represent an average of the results ($n \geq 5$). Thermogravimetric analyses (TGA) were conducted under nitrogen gas flow at a heating rate of 10 ℃/min. The dielectric constants were measured on a CONCEBT 40 broadband dielectric spectroscopy (Novocontrol Technologies, KG, Germany). The breakdown strength was conducted by a dc dielectric strength tester with a sphere–sphere stainless electrode (DH, Shanghai Lanpotronics Co., China) at room temperature.

Results and discussion

In Fig. 2, the absorption band at 1724.4 cm^{-1} is ascribed to the C=O stretching of the –COOH. The peak at 1060.3 cm^{-1} is attributed to the C–O stretching of the C–OH/C–O–C groups.[41, 42] Compared to GO (PPD-GO), CFGO (PPD-CFGO) has weaker C-O stretching absorption, due to a ring opening reaction of epoxy groups catalyzed by HBr, while the intensity of the –OH stretching absorption (3412.3 cm^{-1}) remains constant, indicating the conversion from epoxy to hydroxyl groups. The enhanced C=O absorption of the sample confirms the successful carboxylation of the GO (PPD-GO) and oxalic acid via the esterification reaction. The C=O absorption of PPD-GO is obviously weaker than that of GO while the C-O absorption of PPD-GO is similar, implying that p-phenylenediamine reacted with –COOH but not C-O-C. The characteristic absorption peaks

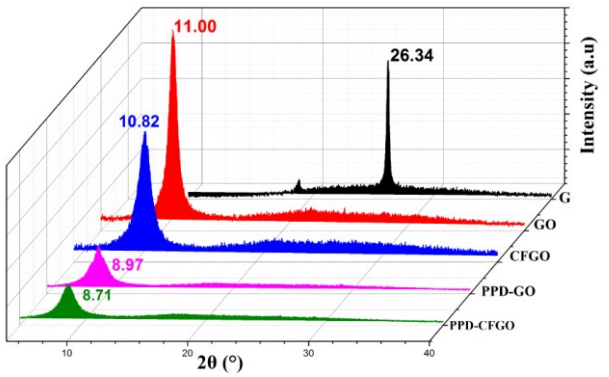

Fig.3 X-Ray diffraction patterns of graphite (G), GO, CFGO, PPD-GO and PPD-CFGO.

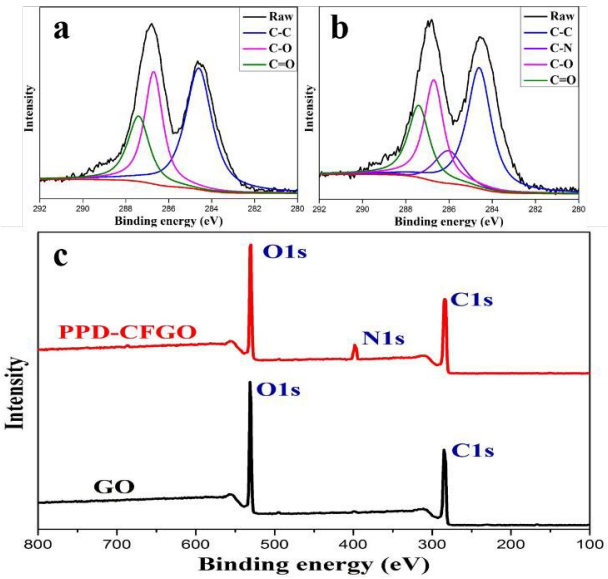

Fig.4 High resolution C1s XPS spectrum of (a) GO and (b) PPD-CFGO; (c) XPS survey scans of GO and PPD-CFGO.

at 1507.8 cm^{-1} is attributed to secondary amine (-NH-) stretching. The characteristic peak of the C-N stretching in the amide of PPD-GO and PPD-CFGO is found at 1242.2 cm^{-1}. The –NH- and C-N stretching absorption of PPD-CFGO are stronger than that of PPD-GO, suggesting that more –COOH groups on CFGO are available to react with $–NH_2$ groups.

The GO XRD patterns exhibit a peak centered at 11.00 °shown in Fig. 3, corresponding to an interlay spacing of 0.803 nm, larger than that of graphite (26.34 °, 0.338 nm) due to the introduction of polar functional groups on carbon sheets.[43] After the esterification, the interlay spacing of the resulting CFGO (10.82 °, 0.817 nm) becomes greater than that of GO due to the introduction of -O-CO-COOH groups on the graphene sheets. The diffraction peak of PPD-GO and PPD-CFGO appears at 8.97 ° (0.985 nm) and 8.71 ° (1.014 nm), respectively, larger than that of GO and CFGO due to the introduction of p-phenylenediamine. The XRD patterns suggest that PPD-modification process provided increased interlayer distance and greater structural heterogeneity.[44]

GO and PPD-CFGO samples are analyzed by XPS. The XPS survey spectra of GO and PPD-CFGO are shown in Fig. 4(c). After functionalization, PPD-CFGO shows a significant increase

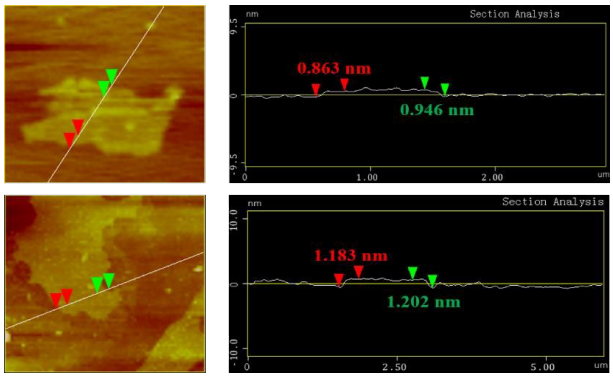

Fig. 5 AFM images of the GO and PPD-CFGO nanosheets.

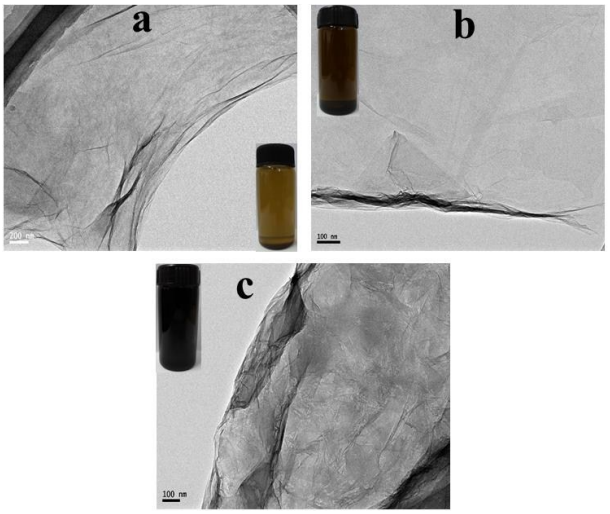

Fig. 6 TEM images of (a) GO, (b) CFGO and (c) PPD-CFGO.

in the N1s peak intensity compared to that of GO. This increase is due to the grafted PPD compounds, confirming the success of the amine modification. Moreover, the C1s XPS spectrum of GO (a) shows three different peaks at 284.6, 286.6 and 287.7 eV, corresponding to the C–C bonds in the aromatic rings, C-O groups, and C=O groups, respectively.[45] After amine modification, the C1s XPS spectrum of PPD-CFGO reveals a significant additional peaks at 285.8 eV, originating from C–N bonds.[28]

In Fig.5, AFM topography indicates the thickness of the GO and PPD-CFGO is about 0.904 nm and 1.192 nm. The lateral dimensions of GO and CFGO are around 1 μm. In Fig.6, ultrathin sheets with wrinkled and silk-like morphology are observed for GO and CFGO.[46, 47] For the PPD-CFGO sample, crumbled and encapsulated morphologies are observed, totally different from that of GO and CFGO, suggesting that the surface properties of the GO sheets are further altered during PPD-modification process,48 extremely likely PPD monomers covalently bonded to the CFGO sheets. After surface modification, the dispersion of PPD-CFGO in DMAc is much better than that of GO and CFGO, and the GO/DMAc (0.2 mg/mL), CFGO/DMAc (1 mg/mL) and PPD-CFGO/DMAc (4 mg/mL) solutions are shown in Fig. 6 (insets).

In the spectrum of pristine graphite (Fig. 7), a prominent G peak at 1575 cm^{-1} corresponding to an E2g mode of graphite represents the in-plane bond-stretching vibration of sp2

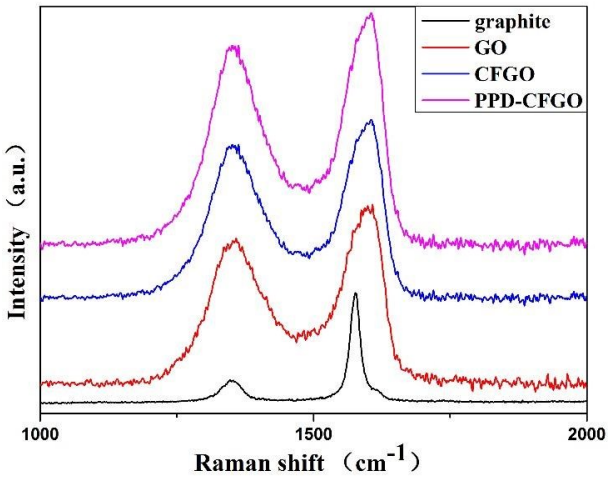

Fig.7 Raman spectra of graphite, GO, CFGO and PPD-CFGO.

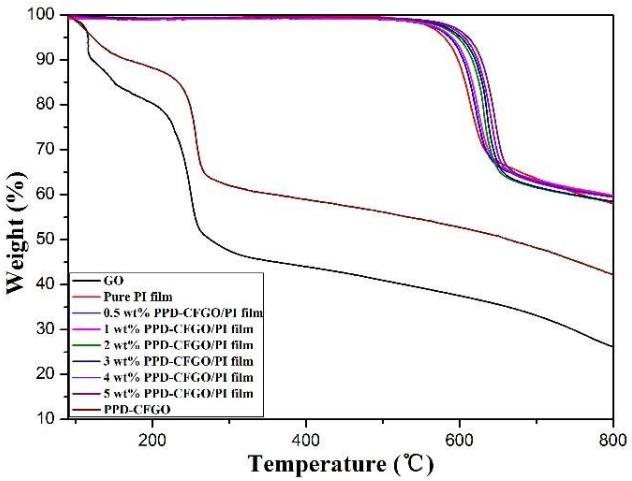

Fig.8 TGA curves of GO, CFGO, pure PI and PPD-CFGO/PI nanocomposite films.

hybridized carbon atoms.[49, 50] The D band at 1350 cm^{-1} is related to the breathing mode of κ-point phonons of A1g symmetric with vibrations of the carbon atoms of dangling bonds in plane terminations of the disordered and defected graphite. The variation of D/G intensity ratio suggests a change in the average size of the sp2 domains.[45] The increase of the D/G ratio of GO (0.82) compared to that of graphite (0.23) indicates that many defects are formed and a high level of disorder is introduced, presumably due to the excessive oxidation.[51] In comparison with the GO, CFGO (0.88) and PPD-CFGO (0.91) has higher D/G ratio, which means the introduction of –O-CO-COOH groups and PPD on the graphene sheets led to the formation of other defects. The D peak becomes stronger and broader during the functionalization process, indicating a high level of disorder.

Thermal stability is one of the important properties for PI-based nanocomposites as they are being used as high-performance engineering plastics. As shown in Fig. 8, the weight loss temperatures of PI, 0.5 wt%, 1 wt%, 2 wt%, 3 wt%, 4 wt% and 5 wt% PPD-CFGO/PI films are 576, 584, 588, 594, 598, 602 and 610 ℃, respectively. The thermal stability of pure PI and its nanocomposites containing different amounts of PPD-CFGO is improved slightly with increasing the graphene composition. Although -CONH- and -COO- groups are not as stable as imide

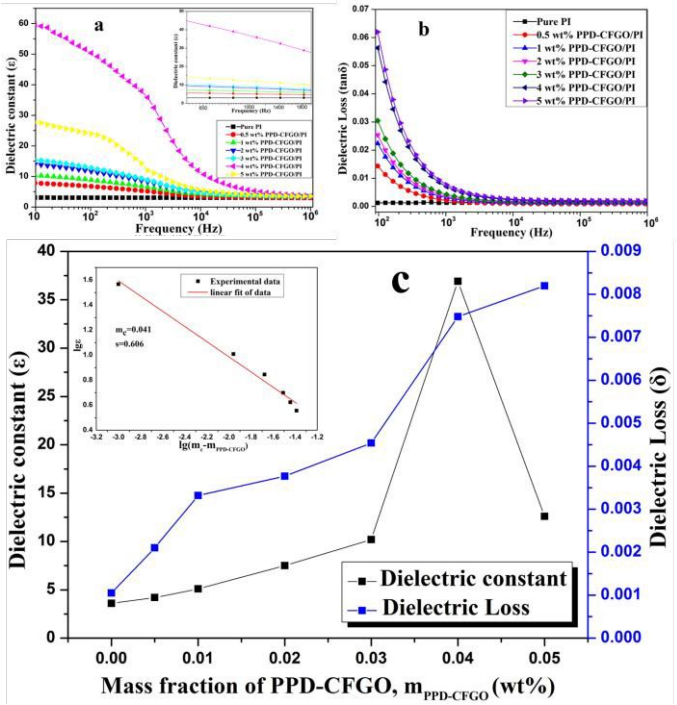

Fig.9 (a) Dielectric constant and (b) dielectric loss as a function of frequency for pure PI and PPD-CFGO/PI films with various amounts of PPD-CFGO at room temperature; (c) Dielectric constant and dielectric loss as a function of the mass fraction of PPD-CFGO at 1 kHz.

groups under high temperature, the thermal stability of the nanocomposites is comparable to that of pure PI.[52, 53] The TGA thermogram of GO includes two stages: first, the weight loss stage starting below 100 ℃ is attributed to the removal of absorbed water; the second weight loss at around 200 ℃ is ascribed to the decomposition of labile oxygen-containing functional groups from the GO layers.[54] For PPD-CFGO, there is a significant weight loss stage at around 200 ℃, similar to GO, indicating that the PPD-CFGO in the composites is reduced during the imidization.

The dielectric constant and dielectric loss of the PPD-CFGO/PI composites as a function of frequency is plotted in Fig. 9 (a) and (b). As summarized in Fig. 9 (c), the permittivity increases dramatically as the PPD-CFGO content approaches and exceeds the percolation threshold, according to the percolation theory. The enhancement of the dielectric constant has been mainly ascribed to the formation of microcapacitor network.[55] The maximum value of the dielectric constant for the nanocomposite with $m_{PPD\text{-}CFGO}$ = 0.04 is 36.9 (Fig. 9 (c)), higher than that of the pure PI polymer (about 3.0) by a factor of ~12.5, while the dielectric loss is 0.0075, demonstrating that PPD-CFGO is dispersed homogeneously in the matrix.[56] The dielectric loss of the PPD-CFGO/PI composites is between 0.0013 and 0.063, which is quite small compared with other traditional percolative composites. The dielectric constant and dielectric loss of 4 wt% PPD-CFGO/PI composites are 36.9 and 0.0075 at 1 kHz, respectively, which indicates the PPD-CFGO/PI composite films are promising polymer-based dielectric with high dielectric constant and ultralow dielectric loss.

As shown in Fig. 10, the SEM images of the fractured surfaces

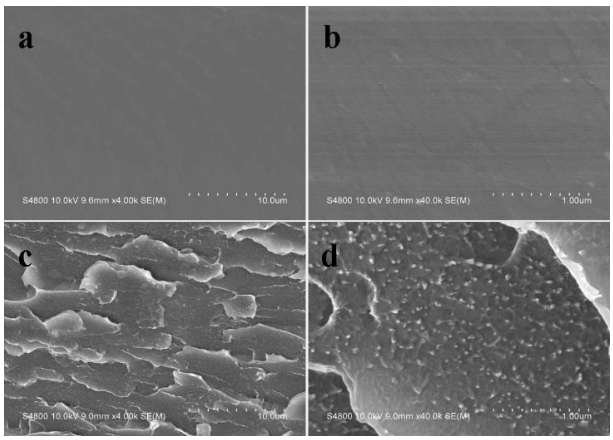

Fig.10 SEM micrographs of the fractured structure of (a) pure PI (×4 k), (b) pure PI (×40 k), (c) 4 wt% GO/PI (×4 k) and (d) 4 wt% PPD-CFGO/PI (×40 k) composite films.

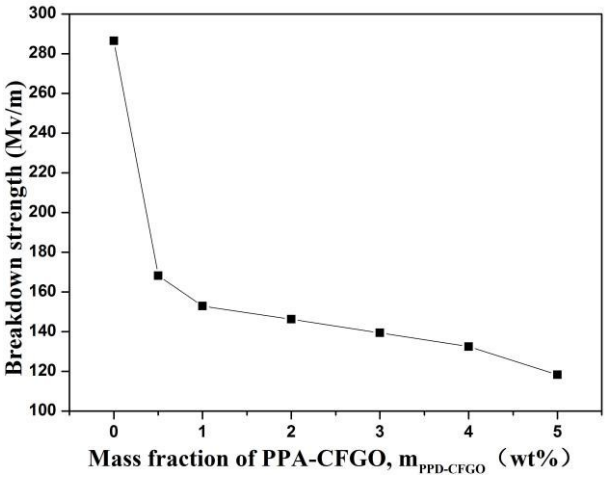

Fig. 11 Breakdown strength of the PPD-CFGO/PI composite films as a function of the PPD-CFGO content.

of the pure PI and 4 wt% PPD-CFGO/PI composite film also prove the excellent dispersion of PPD-CFGO. The fracture surface of pure PI is rather smooth (Fig. 10 (a) and (b)), while rough and ridged for the PPD-CFGO/PI nanocomposite (Fig. 10 c and d), resulting from the 2D geometry of graphene sheets.[57]

For simplification, a mass fraction is used to replace the volume fraction. The percolation threshold can be obtained by equation (1).[58]

$$\varepsilon \propto \left(m_c - m_{PPD-CFGO}\right)^{-s} \text{ for } m_{PPD\text{-}CFGO} < m_c \quad (1)$$

where ε is the permittivity of composites, m_c is the critical mass fraction at the percolation threshold, $m_{PPD\text{-}CFGO}$ is the mass fraction of PPD-CFGO and s is the critical exponent. Furthermore, the experimental values of the permittivity in Fig. 9 (c) are in line with equation (1), with m_c = 0.041 and s = 0.61. As the PPD-CFGO content increases to 0.05, the dielectric constant decreases and the dielectric loss increases simultaneously, mainly due to the destruction of the percolation network and the formation of the conductive network, resulting in the leakage current in the nanocomposites.[59]

For a dielectric materials, in addition to a high dielectric constant, a high breakdown strength is also important, because it determines the operating electric field of the dielectric materials. Fig. 11 presents the breakdown strength of pure PI and PPD-

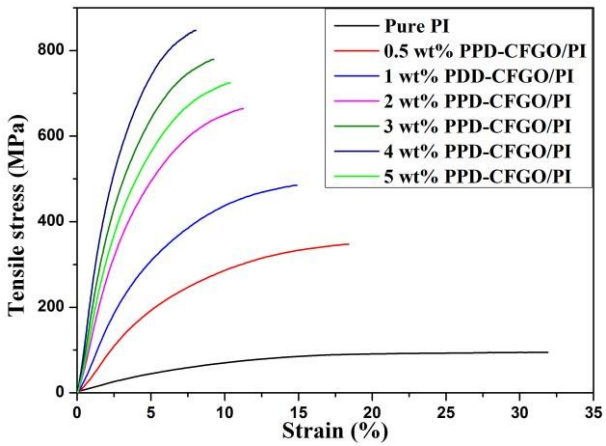

Fig. 12 Stress-strain curves of pure PI films and PPD-CFGO/PI films with various amounts of PPD-CFGO.

Table 1 Summary of mechanical properties of the pure PI and GO/PI films with various amounts of PPD-CFGO.

Sample	Tensile strength/MPa	Tensile modulus/GPa	Elongation at break (%)
Pure PI	94 ±6.1	1.1 ±0.10	32.9 ±11.0
0.5 wt% GO/PI	347 ±5.2	4.0 ±0.09	18.3 ±10.4
1 wt% GO/PI	485 ±7.8	7.3 ±0.12	14.8 ±10.9
2 wt% GO/PI	663 ±6.3	13.1 ±0.13	11.4 ±9.3
3 wt% GO/PI	782 ±11.2	16.9 ±0.18	9.2 ±9.2
4 wt% GO/PI	848 ±10.5	18.5 ±0.14	8.0 ±11.0
5 wt% GO/PI	718 ±9.3	15.7 ±0.12	10.3 ±8.7

CFGO/PI composite films as a function of PPD-CFGO content measured at room temperature. The breakdown strength of the pure PI film is very high (286.5±32.6 MV/m). The addition of a small quantity of PPD-CFGO makes the breakdown strength of 0.5 wt% PPD-CFGO/PI composite films decrease sharply (only 168.2±15.3 MV/m). As the PPD-CFGO content further increases, the breakdown strength of the composite films decrease slowly. However, the breakdown strength of 4 wt% PPD-CFGO/PI composite films still remain at a high level (132.5±9.3 MV/m).

Typical stress-strain curves of pure PI and the PPDGO/PI composites are shown in Fig. 12 and the tensile properties are summarized in Table 1, demonstrating that the PPD-CFGO/PI films exhibit superior mechanical properties compared to pure PI films. The tensile strength of the PPD-CFGO/PI films containing only 0.5 wt% PPD-CFGO is increased up to 347.1 MPa (about 270% greater than that of pure PI films). The increase of the PPD-CFGO content from 0.5 to 5.0 wt% further increases the tensile strength to 848 MPa, along with a dramatic influence on the polymer tensile strength. The tensile modulus shows similar trend as tensile strength with increasing amount of PPD-CFGO. This reinforcement effect from PPD-CFGO can be mainly attributed to its fine dispersion and high orientation in PI, as well as the efficient transfer from the matrix to PPD-CFGO nanoparticles. The strong interactions with the polymer to restrict the movement of the polymer chain effectively leads to the brittleness of composites.[60] Moreover, the elongation at break of composite films is decreased gradually as the PPD-CFGO content increased (as shown in Table 1). However, the tensile strength is 782, 848 and 718 MPa for 3, 4 and 5 wt% of the PPD-CFGO, respectively, a decreasing trend also observed for the tensile modulus. When a critical composition is reached, the distance between any two sheets is so small that Van der Waals forces become predominant, and the sheets agglomerate, thus reducing the PPD-CFGO reinforcement. At lower percentage content, the exfoliated PPD-CFGO produces a significant improvement on the mechanical properties.

In summary, the superior tensile properties of composite films suggest that *in situ* polymerization is an effective method to improve the dispersion and compatibility of PPD-CFGO in PI-composites, and to take advantage of the synergetic benefits of large aspect ratio, homogenous dispersion of the PPD-CFGO within PI, and strong interfacial adhesion due to chemical bonding between PPD-CFGO and the polymer matrix.

Conclusions

We have demonstrated an effective approach using *in situ* polymerization to prepare PPD-CFGO/PI composites with superior performances. Due to the excellent dispersion in DMAc, PPD-CFGO is a versatile starting platform for the *in situ* fabrication of composite films through the grafting of poly(amic acid) onto the PPD-CFGO surface. Combining the ultrahigh contact area and strong interfacial interactions of the PI matrix, the PPD-CFGO nanosheets provide great reinforcement to the PI composites. The PPD-CFGO/PI films, prepared in this work, exhibit a 16.8-time increase in tensile modulus and 800% improvement in tensile strength for a 4 wt% content of PPD-CFGO. The TGA test demonstrated that the composites had good thermal stability below 500 ℃. Furthermore, the dielectric constant of the composite increased as the amount of PPD-CFGO increased, and the percolation was m_c = 0.041. The dielectric constant of the nanocomposite (36.9, $m_{PPD\text{-}CFGO}$ = 0.04) was about 12.5 times higher than that of pure PI polymer, with ultralow dielectric loss (0.0075) and high breakdown strength (132.5±9.3 MV/m). Consequently, *in situ* polymerization provides an effective method to produce PPD-CFGO/PI films, therefore to develop freestanding, lightweight, and strong, graphene-based polyimide composite materials with high dielectric constants, showing promise for a wide range of applications.

Acknowledgements

This work was financially supported by the Basic Innovation Research Program of Science and Technology Commission of Shanghai (13JC1402002), the Natural Science Foundation of Shanghai (12ZR1407900) and the China Scholarship Council.

Notes and references

1. W. Gu, N. Peters and G. Yushin, *Carbon*, 2013, 53, 292-301.
2. M. Zhi, C. Xiang, J. Li, M. Li and N. Wu, *Nanoscale*, 2013, 5, 72-88.
3. Q. Wang and L. Zhu, *Journal of Polymer Science Part B: Polymer Physics*, 2011, 49, 1421-1429.
4. R. Schroeder, L. A. Majewski and M. Grell, *Advanced Materials*, 2005, 17, 1535-1539.
5. M. Rabuffi and G. Picci, *Plasma Science, IEEE Transactions on*, 2002, 30, 1939-1942.
6. J. Park, L. Drahushuk, M. H. Ham, S. W. Kang, J. H. Baik, S. Shimizu, M. S. Strano and C. Song, *Polymer Chemistry*, 2013, 4, 290-295.

7. Y. H. Chou, C. L. Tsai, W. C. Chen and G. S. Liou, *Polymer Chemistry*, 2014, 5, 6718-6727.
8. Y. Bin, K. Oishi, A. Koganemaru, D. Zhu and M. Matsuo, *Carbon*, 2005, 43, 1617-1627.
9. X. Liu, J. Yin, Y. Kong, M. Chen, Y. Feng, Z. Wu, B. Su and Q. Lei, *Thin Solid Films*, 2013, 544, 54-58.
10. A. Alias, Z. Ahmad and A. B. Ismail, *Materials Science and Engineering: B*, 2011, 176, 799-804.
11. K. Abe, D. Nagao, A. Watanabe and M. Konno, *Polymer International*, 2013, 62, 141-145.
12. C. Hamciuc, E. Hamciuc, M. Olariu and R. Ciobanu, *Polymer International*, 2010, 59, 668-675.
13. E. Hamciuc, C. Hamciuc, I. Bacosca, M. Cristea and L. Okrasa, *Polymer Composites*, 2011, 32, 846-855.
14. Q. Chi, J. Sun, C. Zhang, G. Liu, J. Lin, Y. Wang, X. Wang and Q. Lei, *Journal of Materials Chemistry C*, 2014, 2, 172-177.
15. Z. M. Dang, T. Zhou, S. H. Yao, J. K. Yuan, J. W. Zha, H. T. Song, J. Y. Li, Q. Chen, W. T. Yang and J. Bai, *Advanced Materials*, 2009, 21, 2077-2082.
16. Z. M. Dang, Y. H. Lin and C. W. Nan, *Advanced Materials*, 2003, 15, 1625-1629.
17. M. Panda, V. Srinivas and A. K. Thakur, *Applied Physics Letters*, 2011, 99, 042905.
18. C. Huang, Q. M. Zhang and J. Su, *Applied Physics Letters*, 2003, 82, 3502-3504.
19. Y. Chen, B. Lin, X. Zhang, J. Wang, C. Lai, Y. Sun, Y. Liu and H. Yang, *Journal of Materials Chemistry A*, 2014, 2, 14118-14126.
20. L. Rodriguez-Perez, M. a. A. Herranz and N. Martin, *Chemical Communications*, 2013, 49, 3721-3735.
21. J. Wu, W. Pisula and K. Müllen, *Chemical Reviews*, 2007, 107, 718-747.
22. D. Wei and J. Kivioja, *Nanoscale*, 2013, 5, 10108-10126.
23. D. R. Dreyer, S. Park, C. W. Bielawski and R. S. Ruoff, *Chemical Society reviews*, 2010, 39, 228-240.
24. M. Li, X. Huang, C. Wu, H. Xu, P. Jiang and T. Tanaka, *Journal of Materials Chemistry*, 2012, 22, 23477-23484.
25. L. Chu, Q. Xue, J. Sun, F. Xia, W. Xing, D. Xia and M. Dong, *Composites Science and Technology*, 2013, 86, 70-75.
26. X. J. Zhang, G. S. Wang, Y. Z. Wei, L. Guo and M. S. Cao, *Journal of Materials Chemistry A*, 2013, 1, 12115-12122.
27. M. Tian, J. Zhang, L. Zhang, S. Liu, X. Zan, T. Nishi and N. Ning, *Journal of Colloid and Interface Science*, 2014, 430, 249-256.
28. J. Y. Wang, S. Y. Yang, Y. L. Huang, H. W. Tien, W. K. Chin and C. C. M. Ma, *Journal of Materials Chemistry*, 2011, 21, 13569-13575.
29. W. H. Liao, S. Y. Yang, S. T. Hsiao, Y. S. Wang, S. M. Li, H. W. Tien, C. C. M. Ma and S. J. Zeng, *RSC Advances*, 2014, 4, 51117-51125.
30. N. D. Luong, U. Hippi, J. T. Korhonen, A. J. Soininen, J. Ruokolainen, L. S. Johansson, J. D. Nam, L. H. Sinh and J. Seppälä, *Polymer*, 2011, 52, 5237-5242.
31. K. Yang, X. Huang, L. Fang, J. He and P. Jiang, *Nanoscale*, 2014, 6, 14740-14753.
32. M. A. Rafiee, J. Rafiee, Z. Wang, H. Song, Z. Z. Yu and N. Koratkar, *ACS Nano*, 2009, 3, 3884-3890.
33. R. Verdejo, M. M. Bernal, L. J. Romasanta and M. A. Lopez-Manchado, *Journal of Materials Chemistry*, 2011, 21, 3301.
34. X. Zhao, Q. Zhang, D. Chen and P. Lu, *Macromolecules*, 2010, 43, 2357-2363.
35. I. E. Mejias Carpio, J. D. Mangadlao, H. N. Nguyen, R. C. Advincula and D. F. Rodrigues, *Carbon*, 2014, 77, 289-301.
36. H. He, J. Klinowski, M. Forster and A. Lerf, *Chemical Physics Letters*, 1998, 287, 53-56.
37. K. Zhang, L. L. Zhang, X. S. Zhao and J. Wu, *Chemistry of Materials*, 2010, 22, 1392-1401.
38. W. L. Zhang, B. J. Park and H. J. Choi, *Chem Commun (Camb)*, 2010, 46, 5596-5598.
39. Y. Liu, R. Deng, Z. Wang and H. Liu, *Journal of Materials Chemistry*, 2012, 22, 13619.
40. W. S. Hummers, JR. and R. E. Offeman, *Journal of The American Chemical Society*, 1957, 80, 1339.
41. S. Stankovich, R. D. Piner, S. T. Nguyen and R. S. Ruoff, *Carbon*, 2006, 44, 3342-3347.
42. W. Zhang, W. He and X. Jing, *Journal of Physical Chemistry B*, 2010, 114, 10368-10373.
43. O. C. Compton, D. A. Dikin, K. W. Putz, L. C. Brinson and S. T. Nguyen, *Advanced Materials*, 2010, 22, 892-896.
44. Y. Han and Y. Lu, *Carbon*, 2007, 45, 2394-2399.
45. S. Stankovich, D. A. Dikin, R. D. Piner, K. A. Kohlhaas, A. Kleinhammes, Y. Jia, Y. Wu, S. T. Nguyen and R. S. Ruoff, *Carbon*, 2007, 45, 1558-1565.
46. N. D. Luong, N. Pahimanolis, U. Hippi, J. T. Korhonen, J. Ruokolainen, L. S. Johansson, J. D. Nam and J. Seppälä, *Journal of Materials Chemistry*, 2011, 21, 13991.
47. Y. Zhu, S. Murali, W. Cai, X. Li, J. W. Suk, J. R. Potts and R. S. Ruoff, *Advanced Materials*, 2010, 22, 3906-3924.
48. J. Y. Wang, S. Y. Yang, Y. L. Huang, H. W. Tien, W. K. Chin and C. C. M. Ma, *Journal of Materials Chemistry*, 2011, 21, 13569-13575.
49. J. Shen, Y. Hu, M. Shi, X. Lu, C. Qin, C. Li and M. Ye, *Chemistry of Materials*, 2009, 21, 3514-3520.
50. F. Tuinstra and J. L. Koenig, *The Journal of Chemical Physics*, 1970, 53, 1126-1130.
51. X. Zhang, Y. Huang, Y. Wang, Y. Ma, Z. Liu and Y. Chen, *Carbon*, 2009, 47, 334-337.
52. S. H. Yoon, J. H. Park, E. Y. Kim and B. K. Kim, *Colloid and Polymer Science*, 2011, 289, 1809-1814.
53. K. Scully and R. Bissessur, *Thermochimica Acta*, 2009, 490, 32-36.
54. T. Kubota and R. Nakanishi, *Journal of Polymer Science Part B: Polymer Letters*, 1964, 2, 655-659.
55. Z. M. Dang, L. Wang, Y. Yin, Q. Zhang and Q. Q. Lei, *Advanced Materials*, 2007, 19, 852-857.
56. L. Cui, X. Lu, D. Chao, H. Liu, Y. Li and C. Wang, *Physica Status Solidi (a)*, 2011, 208, 459-461.
57. L. B. Zhang, J. Q. Wang, H. G. Wang, Y. Xu, Z. F. Wang, Z. P. Li, Y. J. Mi and S. R. Yang, *Composites Part A: Applied Science and Manufacturing*, 2012, 43, 1537-1545.
58. Y. Chen, Q. Zhuang, X. Liu, J. Liu, S. Lin and Z. Han, *Nanotechnology*, 2013, 24, 245702.
59. F. He, S. Lau, H. L. Chan and J. Fan, *Advanced Materials*, 2009, 21, 710-715.

60. D. Chen, H. Zhu and T. Liu, *ACS applied materials & interfaces*, 2010, 2, 3702-3708.

Preparation and properties of thermostable well-functionalized graphene oxide/polyimide composite films with high dielectric constant, low dielectric loss and high strength via in situ polymerization

Xinliang Fang[a], Xiaoyun Liu[a], Zhong-Kai Cui[b], Jun Qian[*a], Jijia Pan[a], Xinxin Li[a],Qixin Zhuang[*a]

Thermostable well-functionalized graphene oxide/polyimide composites with high dielectric constant and low dielectric loss was obtained at a low percolation threshold.